Journal of Alloys and Compounds 489 (2010) 596–599

Contents lists available at ScienceDirect

Journal of Alloys and Compounds

journal homepage: www.elsevier.com/locate/jallcom

Corrosion behavior of Zr–Cu–Ni–Al bulk metallic glasses in chloride medium

A. Tauseef[a], N.H. Tariq[a,*], J.I. Akhter[b], B.A. Hasan[a], M. Mehmood[c]

[a] Powder Metallurgy Lab, DCME, Pakistan Institute of Engineering and Applied Sciences, P.O. Nilore, Islamabad 45600, Pakistan
[b] Physics Division, Pakistan Institute of Nuclear Science & Technology, P.O. Nilore, Islamabad, Pakistan
[c] National Center for Nano Technology, Pakistan Institute of Engineering and Applied Sciences, P.O. Nilore, Islamabad 45600, Pakistan

ARTICLE INFO

Article history:
Received 22 August 2009
Received in revised form
14 September 2009
Accepted 19 September 2009
Available online 25 September 2009

Keywords:
Amorphous materials
X-ray diffraction
Scanning electron microscopy
Potentiodynamic polarization
Pitting corrosion

ABSTRACT

Polarization and passivation behavior of three Zr-based BMGs, i.e. $Zr_{58.3}Al_{14.6}Ni_{8.3}Cu_{18.8}$, $Zr_{58}Al_{16}Ni_{11}Cu_{15}$ and $Zr_{57.5}Al_{17.5}Ni_{13.8}Cu_{11.3}$ were investigated in 3% NaCl aqueous solution. Electrochemical investigations were carried out by potentiodynamic polarization method at room temperature. The corroded sample surfaces were examined using scanning electron microscope having energy dispersive spectroscopy (EDS) attachment. The results of the present investigation revealed that $Zr_{58}Al_{16}Ni_{11}Cu_{15}$ and $Zr_{57.5}Al_{17.5}Ni_{13.8}Cu_{11.3}$ BMGs having relatively larger supercooled liquid region (ΔT_x) and pitting overpotential (η_{pit}) values exhibit low corrosion current density (i_{corr}) and corrosion penetration rate (CPR) values.

1. Introduction

Bulk metallic glasses (BMGs) have attracted increasing attention in the past decade because of their importance in both fundamental science and engineering applications [1,2]. BMGs have unique characteristics (high mechanical strength, high elastic limit, good corrosion resistance, etc.), which cannot be obtained for conventional materials [3]. The structural disorderness, chemical homogeneity and absence of nucleation sites for corrosion such as grain boundaries or dislocations make BMGs good corrosion resistant as compared to their crystalline counterparts.

Zr–Al–Ni–Cu bulk amorphous alloys belong to one of the best glass-forming systems and can be cast at relatively low cooling rate in order to solidify as a glass [4]. They exhibit excellent mechanical properties, i.e. extremely high yield strength combined with a relatively low Young's modulus and high elastic limit which make them a suitable candidate for many hi-tech industrial applications [5,6]. For instance, Zr-based BMGs have been successfully used for preparing diaphragm of pressure sensor device exhibiting 3.8 times higher sensitivity than that of the sensor with the conventional SUS 630 diaphragm [6]. In addition, these BMGs have also been proposed for some biomedical applications [7,8]. For example, it can be used for making bone fracture fixation and hip arthroplasty components where a low modulus comparable to bone is critical to avoid stress shielding. Furthermore, the superior strength would permit a smaller, less intrusive device that would be capable of withstanding the large forces generated within the skeletal system of the human body [7]. However, the applications of the bulk amorphous alloys require high chemical stability in various environments in order to ensure its lifetime. Zr-based BMGs exhibit an excellent passivation behavior in halide-free solutions at room temperature owing to the properties of their valve metal components, e.g. Zr, Al, Ti, etc. [9]. On the other hand, they are strongly susceptible to chloride-induced pitting corrosion [10–12]. Thus, it is of interest to improve corrosion resistance of BMGs in chloride-containing solutions and understanding the pitting mechanism through careful composition choices. In the present work, corrosion behavior of three Zr-based BMGs is investigated in 3% NaCl aqueous solution. It was observed that the alloys with larger supercooled liquid region showed good corrosion resistance.

2. Experimental

Buttons of $Zr_{58.3}Al_{14.6}Ni_{8.3}Cu_{18.8}$, $Zr_{58}Al_{16}Ni_{15}Cu_{11}$ and $Zr_{57.5}Al_{17.5}Ni_{13.8}Cu_{11.2}$ were prepared by arc melting of high purity Zr (4N), Cu (4N), Ni (4N) and Al (4N) under Ti-getter purified argon atmosphere. The samples were remelted four times to improve homogeneity. These buttons were finally remelted and suction-cast into plate shape in copper dies. The dimension of plates was 50 mm × 8 mm × 2 mm respectively. Each plate was cut into a sample with the dimension 8 mm × 4 mm × 2 mm for electrochemical characterization. The samples were metallographically polished to a 0.5 μm diamond paste finish at the same experimental conditions and mirror like finished surface was examined under optical microscope. In addition to that samples were examined using SEM and a typical BMGs featureless morphology was observed. Low temperature differential scanning

* Corresponding author. Tel.: +92 51 220738.
E-mail address: naeem421@hotmail.com (N.H. Tariq).

0925-8388/$ – see front matter © 2009 Elsevier B.V. All rights reserved.
doi:10.1016/j.jallcom.2009.09.119

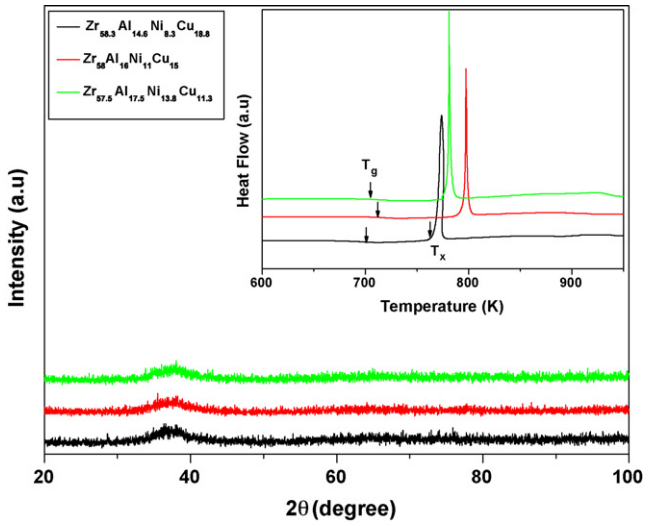

Fig. 1. XRD patterns and low temperature DSC (inset) of as-cast $Zr_{58.3}Al_{14.6}Ni_{8.3}Cu_{18.8}$, $Zr_{58}Al_{16}Ni_{15}Cu_{11}$ and $Zr_{57.5}Al_{17.5}Ni_{13.8}Cu_{11.2}$ bulk amorphous alloys.

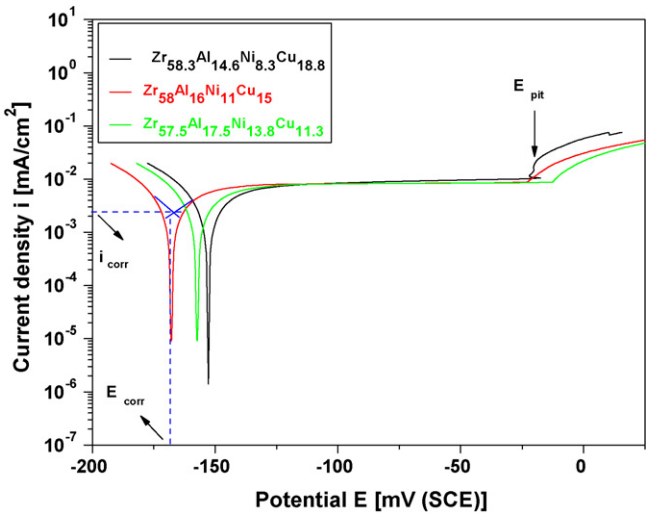

Fig. 2. Potentiodynamic polarization plots of as-cast $Zr_{58.3}Al_{14.6}Ni_{8.3}Cu_{18.8}$, $Zr_{58}Al_{16}Ni_{15}Cu_{11}$ and $Zr_{57.5}Al_{17.5}Ni_{13.8}Cu_{11.2}$ bulk amorphous alloys in 0.5 M NaCl solution.

calorimetry (DSC) was carried out using TA INSTRUMENTS/DSC-Q100 at heating rate of 20 K/min to evaluate thermal parameters. X-ray diffraction (XRD) of all three alloys was conducted, by Shimadzu XRD-6000 using Cu $K\alpha_1$ radiation ($\lambda = 1.54060$ Å) to confirm the amorphous nature of these alloys.

The electrochemical characteristics of the alloys were investigated using anodic polarization curves that were measured by potentiodynamic method with a potential sweep rate of 5 mV/s. The potentiodynamic polarization tests were performed using Amel model 7050 Potentiostat/Galvanostat & Junior Assist software attached with typical three-electrode system, i.e. a stationary sample electrode, a platinum counter electrode and saturated calomel electrode (SCE). The electrolyte used was 3% NaCl, which was prepared from reagent grade chemical and distilled water. Before starting polarization scan, each corrosion sample was allowed to stabilize in the electrolyte for about 10 min till the open circuit potentials become almost steady. The corroded samples were examined under scanning electron microscope and analysis was performed using EDS.

3. Results and discussions

Fig. 1 shows the X-ray diffraction (XRD) patterns of the as-cast alloys. A single amorphous phase was achieved in the samples, as evidenced by a broad diffraction maximum in their XRD pattern. Low temperature DSC plots of the alloys at heating rate of 20 K/min are shown as an inset of Fig. 1. All three DSC traces show a single endothermic peak, indicating the glass transition T_g, and an exothermic peak suggesting single stage crystallization reaction in the alloys. This also confirms amorphous nature of the alloys. The glass transition temperature (T_g), the onset temperature of crystallization (T_x) and the resulting temperature of supercooled liquid region (ΔT_x) are listed in Table 1.

The corrosion behavior of the as-cast $Zr_{58.3}Al_{14.6}Ni_{8.3}Cu_{18.8}$, $Zr_{58}Al_{16}Ni_{15}Cu_{11}$ and $Zr_{57.5}Al_{17.5}Ni_{13.8}Cu_{11.2}$ bulk amorphous alloys was characterized by potentiodynamic polarization in 3% NaCl solution open to air at 298 K. The anodic and cathodic polarization curves are shown in Fig. 2. It can be seen that all BMGs showed quite similar polarization behavior, i.e. they spontaneous passivated with a similar corrosion potential of about −128 mV and very low passive current densities ranging from 5.8 to 7.8 μA/cm^2. This indicates that highly protective and uniform surface film has been immediately formed on the surface of all three BMGs exposed to 3% NaCl solution [13], which suggests high corrosion resistant nature of the alloys. All the three alloys exhibited wide passive region before trans-passive pitting corrosion occurred. It is clear from Fig. 2 that $Zr_{58.3}Al_{14.6}Ni_{8.3}Cu_{18.8}$ and $Zr_{58}Al_{16}Ni_{11}Cu_{15}$ BMGs showed much higher pitting potential as compared to that of $Zr_{57.5}Al_{17.5}Ni_{13.8}Cu_{11.3}$. Table 2 summarizes electrochemical corrosion properties derived from the potentiodynamic polarization tests of BMGs under study. The pitting overpotential ($\eta_{pit} = E_{pit} - E_{corr}$) is an important parameter to measure resistance to localized pitting corrosion. Smaller the value is, the easier is the pit initiation and vice versa. This is also evident from Fig. 2, i.e. $Zr_{58.3}Al_{14.6}Ni_{8.3}Cu_{18.8}$ BMG (with small η_{pit}) showing sudden increase of anodic current at pitting potential (E_{pit}) in comparison to $Zr_{58}Al_{16}Ni_{11}Cu_{15}$ and $Zr_{57.5}Al_{17.5}Ni_{13.8}Cu_{11.3}$ (having relatively larger η_{pit}) with gradual increase of anodic current. The corrosion rate under natural corrosion conditions, i.e. at corrosion potential (E_{corr}), is related to the corrosion current density (i_{corr}), which is calculated by Tafel extrapolation method schematically shown in Fig. 2. The corrosion penetration rate (CPR, μm/year) is then calculated by application of Faraday's law:

$$CPR = \frac{0.327(Mi_{corr})}{m\rho}$$

where M (g/mol), m and ρ (g/cm^3) are the atomic fraction weighted values of atomic weight, ion valence and density respectively, for the alloy elements, and i_{corr} (mA/m^2) is the corrosion current density [11]. It was observed that $Zr_{58}Al_{16}Ni_{11}Cu_{15}$ and $Zr_{57.5}Al_{17.5}Ni_{13.8}Cu_{11.3}$ BMGs having relatively larger ΔT_x and η_{pit} values exhibited low i_{corr} and CPR values.

To better understand the chloride-induced localized corrosion mechanism, SEM was employed to investigate the morphologies of the samples after polarization tests. Fig. 3(a–c) shows the corroded regions for $Zr_{58.3}Al_{14.6}Ni_{8.3}Cu_{18.8}$, $Zr_{58}Al_{16}Ni_{11}Cu_{15}$ and $Zr_{57.5}Al_{17.5}Ni_{13.8}Cu_{11.3}$ respectively. Pitting corrosion can be clearly observed. It is also very clear that $Zr_{58.3}Al_{14.6}Ni_{8.3}Cu_{18.8}$ showed less resistance to pitting corrosion as compared to $Zr_{58}Al_{16}Ni_{11}Cu_{15}$ and $Zr_{57.5}Al_{17.5}Ni_{13.8}Cu_{11.3}$ which is in agreement with potentiodynamic polarization results as discussed earlier, i.e. $Zr_{58.3}Al_{14.6}Ni_{8.3}Cu_{18.8}$ BMG having relatively small ΔT_x and η_{pit} values exhibited high i_{corr} and CPR values. It can be seen that pits having different size and morphology are distributed homoge-

Table 1
Thermal parameters obtained from DSC for as-cast alloys at heating rate of 20 K/min.

Sample	T_g (K)	T_x (K)	ΔT_x (K)
$Zr_{58.3}Al_{14.6}Ni_{8.3}Cu_{18.8}$	701	762	61
$Zr_{58}Al_{16}Ni_{11}Cu_{15}$	713	793	80
$Zr_{57.5}Al_{17.5}Ni_{13.8}Cu_{11.3}$	703	776	73

Table 2
Electrochemical corrosion properties derived from the potentiodynamic polarization tests of as-cast $Zr_{58.3}Al_{14.6}Ni_{8.3}Cu_{18.8}$, $Zr_{58}Al_{16}Ni_{11}Cu_{15}$ and $Zr_{57.5}Al_{17.5}Ni_{13.8}Cu_{11.3}$ BMGs in 3% NaCl.

BMGs composition	E_{corr} (mV)	i_{corr} (μA/cm^2)	CPR (μm/year)	E_{pit} (mV)	η_{pit} or ($E_{pit} - E_{corr}$) (mV)
$Zr_{58.3}Al_{14.6}Ni_{8.3}Cu_{18.8}$	−153.92	2.50	9.11	−20.27	133.65
$Zr_{58}Al_{16}Ni_{11}Cu_{15}$	−167.95	1.96	7.09	−22.00	145.95
$Zr_{57.5}Al_{17.5}Ni_{13.8}Cu_{11.3}$	−158.08	2.03	7.59	−12.3	145.78

neously on the surface of $Zr_{58.3}Al_{14.6}Ni_{8.3}Cu_{18.8}$. On the other hand corroded surface of $Zr_{58}Al_{16}Ni_{11}Cu_{15}$ and $Zr_{57.5}Al_{17.5}Ni_{13.8}Cu_{11.3}$ showed inhomogeneous distribution of pits, which are relatively much smaller in size. Fig. 4(a–c) shows high magnification SEM images of marked portions of $Zr_{58.3}Al_{14.6}Ni_{8.3}Cu_{18.8}$, $Zr_{58}Al_{16}Ni_{11}Cu_{15}$ and $Zr_{57.5}Al_{17.5}Ni_{13.8}Cu_{11.3}$ in Fig. 3(a–c) respectively. It is noted that passive film of $Zr_{58.3}Al_{14.6}Ni_{8.3}Cu_{18.8}$ cracked due to the heavy attack of corrosion in 3% NaCl solution (Fig. 4(a)) while $Zr_{58}Al_{16}Ni_{11}Cu_{15}$ and $Zr_{57.5}Al_{17.5}Ni_{13.8}Cu_{11.3}$ showed smooth passive film (not shown here). In all samples, inside each of the pits a typical "honeycomb like" micromesh structure was formed, and corrosion products (bright product zone) were found around the wall of the pits as shown in Fig. 4(a–c) [13,14]. The various zones of pitted area were identified as shown in Fig. 4. EDS analysis was carried out to quantify the elemental distribution on these zones.

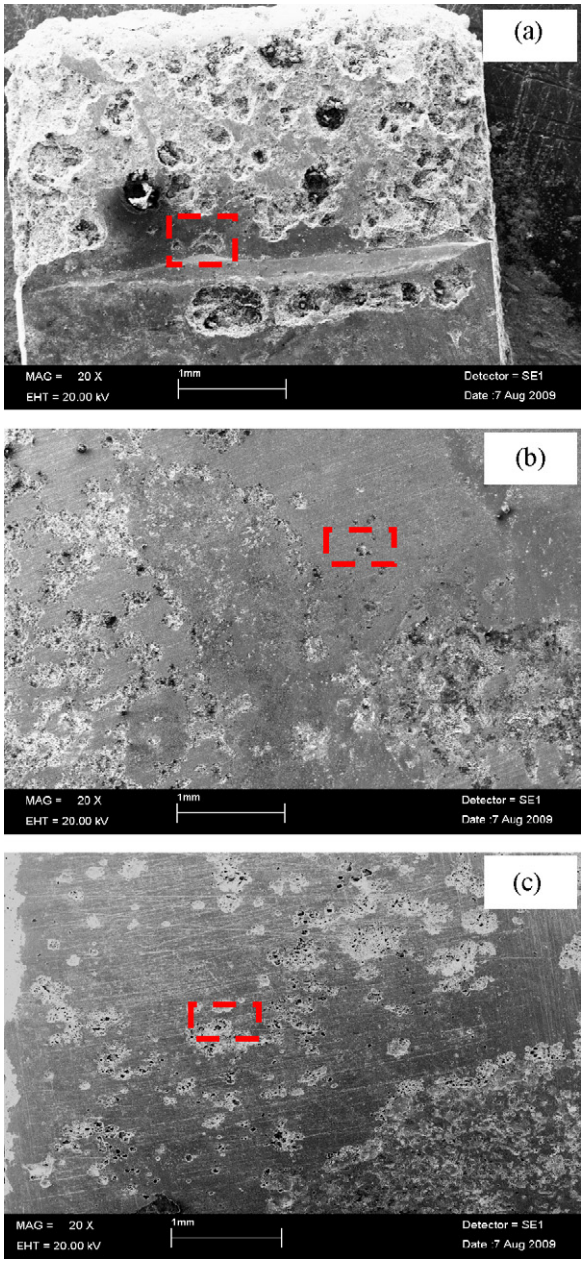

Fig. 3. SEM images of the corroded surface of the three bulk amorphous alloys: (a) $Zr_{58.3}Al_{14.6}Ni_{8.3}Cu_{18.8}$, (b) $Zr_{58}Al_{16}Ni_{15}Cu_{11}$ and (c) $Zr_{57.5}Al_{17.5}Ni_{13.8}Cu_{11.2}$.

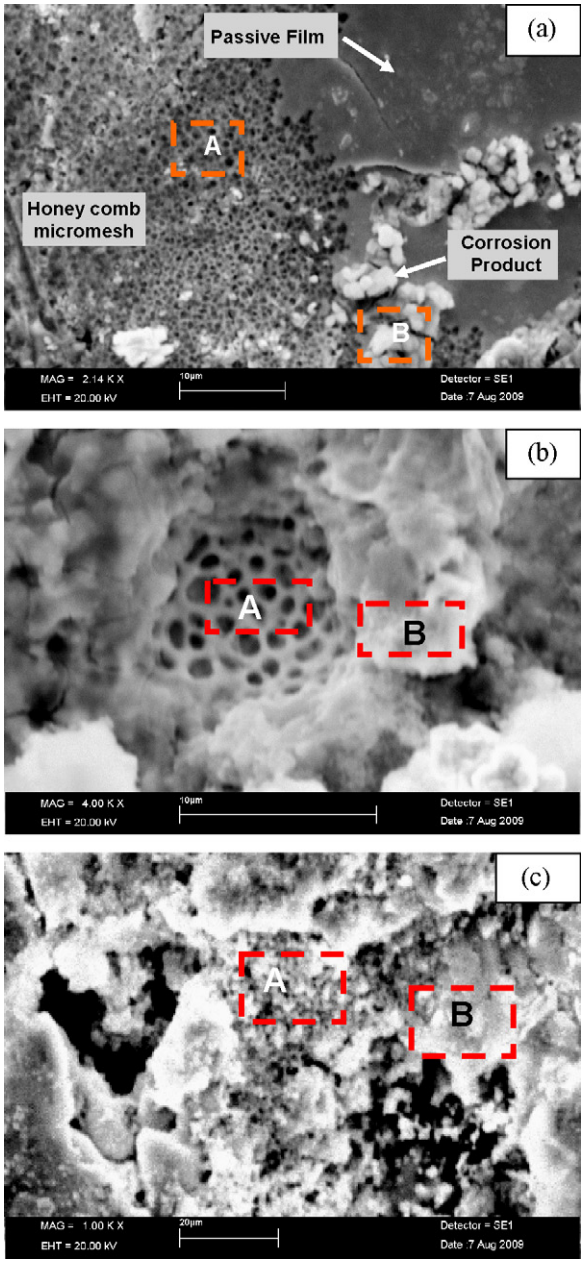

Fig. 4. High magnification characteristic morphologies of pits generated at the corroded surface of (a) $Zr_{58.3}Al_{14.6}Ni_{8.3}Cu_{18.8}$, (b) $Zr_{58}Al_{16}Ni_{15}Cu_{11}$ and (c) $Zr_{57.5}Al_{17.5}Ni_{13.8}Cu_{11.2}$.

Table 3
Composition data at micropores and white corrosion product by EDS for as-cast $Zr_{58.3}Al_{14.6}Ni_{8.3}Cu_{18.8}$, $Zr_{58}Al_{16}Ni_{11}Cu_{15}$ and $Zr_{57.5}Al_{17.5}Ni_{13.8}Cu_{11.3}$ BMGs.

Sample	Region	Zr	Cu	Ni	Al	O	Cl
$Zr_{58.3}Al_{14.6}Ni_{8.3}Cu_{18.8}$	A	18.66	48.21	3.22	5.91	3.4	21.06
	B	26.32	2.3	3.3	1.4	50.22	16.46
$Zr_{58}Al_{16}Ni_{11}Cu_{15}$	A	22.24	47.78	8.77	4.28	12.85	4.09
	B	15.32	1.33	2.33	1.4	70.22	9.76
$Zr_{57.5}Al_{17.5}Ni_{13.8}Cu_{11.3}$	A	26.2	42.03	11.10	7.29	10.8	2.45
	B	19.32	5.33	3.38	2.76	65.44	3.77

Two locations were marked as A and B in Fig. 4(a–c), representing honeycomb mesh and the precipitated corrosion product formed during polarization. The EDS results are shown in Table 3. It was observed that Zr, Al and Ni contents were decreased due to the preferential dissolution while the Cu content stayed higher. The composition of micromesh honeycomb (region A) in all the three BMG samples was mainly composed of Cu element. This is in agreement with that Cu dissolved and redeposit in the pits [14]. At the "bright product" zone (region B), the oxygen concentration is significantly high indicating the formation of oxide corrosion product by all components precipitated around the pit area. From Table 3, it is clear that preferential dissolution of Zr, Al and Ni contents in case of $Zr_{58.3}Al_{14.6}Ni_{8.3}Cu_{18.8}$ is larger as compared to $Zr_{58}Al_{16}Ni_{11}Cu_{15}$ and $Zr_{57.5}Al_{17.5}Ni_{13.8}Cu_{11.3}$ indicating its relatively higher susceptibility to pitting corrosion.

The difference in the pitting susceptibility arises due to chemically inhomogeneous cluster packing (related to the glass-forming ability of the alloy, i.e. ΔT_x) as well as nanometric physical defects formed during casting stage. It is suggested from above findings that $Zr_{58.3}Al_{14.6}Ni_{8.3}Cu_{18.8}$ having small ΔT_x may contain slightly larger chemically inhomogeneous cluster packing as well as higher nanometric physical defect density which provide an interface for the adsorption of chloride ions. This is also evident by high Cl content in both regions of $Zr_{58.3}Al_{14.6}Ni_{8.3}Cu_{18.8}$.

4. Conclusions

Corrosion behavior of three Zr-based BMGs, i.e. $Zr_{58.3}Al_{14.6}Ni_{8.3}Cu_{18.8}$, $Zr_{58}Al_{16}Ni_{11}Cu_{15}$ and $Zr_{57.5}Al_{17.5}Ni_{13.8}Cu_{11.3}$ was investigated in 3% NaCl aqueous solution. It was observed that $Zr_{58}Al_{16}Ni_{11}Cu_{15}$ and $Zr_{57.5}Al_{17.5}Ni_{13.8}Cu_{11.3}$ BMGs having relatively larger ΔT_x and η_{pit} values exhibited low i_{corr} and CPR values. It is concluded that $Zr_{58.3}Al_{14.6}Ni_{8.3}Cu_{18.8}$ having small ΔT_x may contain slightly larger chemically inhomogeneous cluster packing as well as higher nanometric physical defect density, which facilitate the adsorption of destructive chloride ions in the amorphous matrix and hence reducing the corrosion resistance.

References

[1] A. Inoue, T. Zhang, T. Masumoto, Mater. Trans. JIM 31 (1990) 104.
[2] A. Peker, W.L. Johnson, Appl. Phys. Lett. 63 (1993) 2343.
[3] J.H. Kim, C. Lee, D.M. Lee, J.H. Sun, S.Y. Shin, J.C. Bae, Mater. Sci. Eng. A 449–451 (2007) 872.
[4] A. Inoue, T. Nakamura, T. Sugita, T. Zhang, T. Masumoto, Mater. Trans. JIM 34 (1993) 351.
[5] A. Inoue, X.M. Wang, W. Zhang, Rev. Adv. Mater. Sci. 18 (2008) 1–9.
[6] N. Nishiyama, K. Amiya, A. Inoue, J. Non-Cryst. Solids 353 (2007) 3621.
[7] M.L. Morrison, R.A. Buchanan, R.V. Leon, C.T. Liu, B.A. Green, P.K. Liaw, J.A. Horton, J. Biomed. Mater. Res. A 74A (2005) 430–431.
[8] S. Hiromoto, A.P. Tsai, M. Sumita, T. Hanawa, Corros. Sci. 42 (2000) 1651.
[9] A. Gebert, K. Buchholz, A. Leonhard, K. Mummert, J. Eckert, L. Schultz, Mater. Sci. Eng. A 267 (1999) 294.
[10] U. Kamachi Mudali, S. Baunack, J. Eckert, L. Schultz, A. Gebert, J. Alloys Compd. 377 (2004) 290.
[11] W.H. Peter, R.A. Buchanan, C.T. Liu, P.K. Liaw, M.L. Morrison, J.A. Horton, C.A. Carmichael, J.L. Wright, Intermetallics 10 (2002) 1157–1159.
[12] S. Pang, T. Chang, K. Asami, A. Inoue, J. Mater. Res. 18 (2003) 1652.
[13] L. Liu, C.L. Qiu, H. Zou, K.C. Chan, J. Alloys Compd. 399 (2005) 146.
[14] U. Kamachi Mudali, S. Baunack, J. Eckert, L. Schultz, A. Gebert, J. Alloys Compd. 377 (2004) 296.